



Influence of annealing time on electrochemical hydrogen storage properties of $\text{La}_{0.5}\text{Nd}_{0.05}\text{Sm}_{0.3}\text{Mg}_{0.15}\text{Ni}_{3.5}$ alloys

Liqiang Ji¹ · Xin Zhao² · Dandan Ke²

© Springer Nature Switzerland AG 2018

Abstract

$\text{La}_{0.5}\text{Nd}_{0.05}\text{Sm}_{0.30}\text{Mg}_{0.15}\text{Ni}_{3.5}$ alloy was prepared by induction melting followed by annealing treatments. The effect of annealing time on the microstructure and electrochemical performances were investigated. Rietveld analyses results show that all the alloys mainly consist of major A_2B_7 and A_5B_{19} phases and residual AB_5 phase. $\text{Pr}_5\text{Co}_{19}$ -type phase disappears with annealing treatment time prolonged to 9 h. The A_2B_7 phase abundance first increases and then decreases with the increasing annealing time from 6 to 12 h while A_5B_{19} and AB_5 phase abundances show the reverse trend. Moreover, a -axis parameter, c -axis and unit cell volume of the phases remain almost unchanged with prolonging the holding time. The activation properties of the alloy electrodes have not been affected by annealing time. The maximum discharge capacity of alloy electrodes monotonically increase from 326.5 mAh g^{-1} ($t=6 \text{ h}$) to 362.2 mAh g^{-1} ($t=12 \text{ h}$). HRD_{2000} decreases from 63.8% ($x=0$) to 55.5% ($x=0.20$), which is determined by hydrogen diffusion coefficient. The cycling capacity retention rate at the 200th cycle monotonically increases from 67.0% ($x=0$) to 70.6% ($x=0.30$), which should be ascribed to the improvement of corrosion resistance of alloy electrodes in the charging/discharging cycle.

Keywords La–Mg–Ni-based alloy · Electrochemical properties · Annealing treatment · Phase structure · Ni–MH battery

1 Introduction

Nickel/metal hydride (Ni–MH) battery, using hydrogen storage alloy as its negative material with the merit of pollution-free and superior performances, has got more and more attention in order to meet the urgent needs of high performance of secondary batteries and for environmental protection. To date, AB_5 -type alloys have been widely used in almost all commercial Ni–MH batteries because of their good overall electrode properties [1]. However, the electrochemical capacity of AB_5 -type alloys limited by the single CaCu_5 -type hexagonal structure is needed to be improved [2]. Meanwhile, the energy densities of the Ni–MH batteries cannot compete favorably with some other advanced secondary batteries. Therefore, it is urgently needed for new types of alloys to replace the conventional rare-earth-based AB_5 -type alloys with higher

energy densities, faster activation, better rate discharge-abilities, and lower cost are [3].

Recently, several new and good hydrogen storage alloys were reported. The striking studies are a new family of alloys composed of the AB_3 - and A_2B_7 -type rare earth–magnesium–nickel-based intermetallics [4]. RE–Mg–Ni-based hydrogen storage alloys have been considered as a promising candidate for the negative electrode materials of nickel/metal hydride batteries to substitute for AB_5 -type alloys due to their higher discharge capacity (380–410 mAh/g) [5–7]. It was reported that the discharge capacity of the $\text{La}_{0.7}\text{Mg}_{0.3}\text{Ni}_{2.8}\text{Co}_{0.5}$ alloy reached 410 mA h g^{-1} [8], which was 1.3 times that of AB_5 -type alloys. However, due to the corrosion and dissolution of the hydrogen absorbing elements (RE and Mg) in the KOH solution and the pulverization of the alloy particles during electrochemical charging/discharging cycling, the cycling

✉ Xin Zhao, fatcatzx@163.com | ¹Inner Mongolia Rare Earth Ovonic Metal Hydride Co. Ltd., Baotou 014030, China. ²College of Materials and Metallurgy, Inner Mongolia University of Science and Technology, Baotou 014010, China.

stability of RE–Mg–Ni-based alloy electrodes is poor, which restrains their practical applications and industrialization [9, 10]. Moreover, with the rapid development of electric equipments, the hydrogen storage alloys used as the materials of nickel/metal hydride batteries are required to possess faster activation, better rate capability and lower cost [11, 12].

Generally, annealing treatment has been reported to be an effective way to improve overall properties of the alloys. Sakai et al. [13] investigated that annealing treatment on the rare-earth-based hydrogen storage alloys could decrease crystal defects and increase composition homogenization, and consequently enhance the discharge capacity and cyclic stability of the alloys. Hu [14] and [15] also investigated that the annealing treatments contributed to improve the electrochemical cycling stability of Co-free La_2MgNi_9 alloy and $\text{La}_{1.8}\text{Ti}_{0.2}\text{MgNi}_{8.9}\text{Al}_{0.1}$ alloy, respectively. Pan et al. studied the La–Mg–Ni–Co system hydrogen storage alloys, and reported that annealing significantly prolonged the cycle life of $\text{La}_{0.67}\text{Mg}_{0.33}\text{Ni}_{2.5}\text{Co}_{0.5}$ [16] and $\text{La}_{0.7}\text{Mg}_{0.3}\text{Ni}_{2.45}\text{Co}_{0.75}\text{Mn}_{0.1}\text{Al}_{0.2}$ [17] alloy electrodes due to composition homogenization. Wang [18] investigated the effect of annealing time on the structure and electrochemical properties of $\text{La}_{0.72}\text{Nd}_{0.08}\text{Mg}_{0.2}\text{Ni}_{3.4}\text{Al}_{0.1}$ alloys. Lengthening annealing time at 1173 K notably increases discharge capacity and cyclic stability and promotes the formation of Gd_2Co_7 -type phase, meanwhile, the abundance of Gd_2Co_7 -type phase obviously increases with the increase of annealing time. Obviously, annealing treatment is effective to enhance discharge capacity and improve cycling stability of La–Mg–Ni alloy. However, most investigations focused on the effect of annealing temperature, few reports dealt with the effect of annealing time.

In this work, based on the above reasons, a systemic about the effects of the annealing time on the microstructure and electrochemical performances of $\text{La}_{0.5}\text{Nd}_{0.05}\text{Sm}_{0.30}\text{Mg}_{0.15}\text{Ni}_{3.5}$ alloy was investigated. It is expected that the overall electrochemical performances of $\text{La}_{0.5}\text{Nd}_{0.05}\text{Sm}_{0.30}\text{Mg}_{0.15}\text{Ni}_{3.5}$ alloy electrodes can be improved simultaneously with the different annealing time, particularly the maximum discharge capacity and cycling stability.

2 Experimental procedures

2.1 Alloys preparation

$\text{La}_{0.5}\text{Nd}_{0.05}\text{Sm}_{0.30}\text{Mg}_{0.15}\text{Ni}_{3.5}$ alloy was synthesized by induction melting of the metal elements (La, Nd, Sm, Ni and Mg) in argon atmosphere. Then the ingot was annealed by using vacuum heat-treating furnace. Before heating, the sample cell was vacuumized until pressure is less than

10 Pa and then the argon was charged into the sample cell until the pressure was 0.8 MPa. The samples were heated from room temperature to 1048 K at the rate of 10 K min^{-1} and then kept in 1048 K for 6 h, 9 h and 12 h, respectively. Afterwards, the furnace cooling to room temperature air-cooled under an argon atmosphere.

2.2 Microstructure analysis

The alloy powders of measuring electrodes were obtained by grinding the inner part of alloy ingots in the Ar atmosphere. Sample powders of ~ 300 mesh size were used for X-ray diffraction (XRD) measurement, which was carried out on X'pert PROMPD X-ray diffractometer with Cu K α radiation in the range from 20° to 80° with $0.02^\circ\text{ min}^{-1}$, and the results were analyzed by means of Rietveld method using the Maud software.

2.3 PCT measurements

The hydrogen storage properties of the alloys were studied by using pressure-composition-temperature (PCT) (made by Suzuki Shokan in Japan). Before the PCT measurement, the samples were evacuated at 354 K for 2 h. Then the alloys were hydrided at ~ 2 MPa H_2 pressure and then dehydrided to ~ 0.001 MPa. The hydriding/dehydriding process was repeated for 5 times to activate the alloys. After activation, the PCT curves were measured at 314 K. The delay time was 180 s and maximum pressure was 2 MPa.

2.4 Electrochemical measurements

The electrodes for testing were prepared by mixing mechanically the alloy powders (0.1500 g) of 200–400 mesh and the Ni powders (0.7500 g) in the weight ratio 1:5 and cold pressed into pellets (10 mm) at 15 MPa with maintain pressure 2–3 min. Electrochemical measurements were performed at 298 K in a standard tri-electrode system, consisting of a working electrode (metal hydride), a counter electrode ($\text{Ni}(\text{OH})_2/\text{NiOOH}$), and a reference electrode (Hg/HgO) with 6 mol L^{-1} KOH solution as electrolyte. Each electrode was charged for 7 h at 80 mA g^{-1} and discharged to -0.6 V versus Hg/HgO at 80 mA g^{-1} at 298 K. After every charging/discharging, standing for 10 min. In evaluating the high-rate dischargeability, discharge capacity of the alloy electrodes at different discharge current density was measured. The high-rate dischargeability (HRD, %) was defined as

$$\text{HRD} = C_d/C_{\text{max}} \times 100\% \quad (1)$$

where C_d was the discharge capacity at the discharge current density I_d ($I_d = 80, 400, 1200$ and 2000 mA g^{-1} ,

respectively), and C_{\max} was the maximum discharge capacity at the discharge current density of 80 mA g^{-1} .

The electrochemical impedance spectrum, the linear polarization curves and the potential-step measurements were performed on a PARSTAT 2273 Advanced Potentiostat/Galvanostat station, respectively. At 50% depth of discharge (DOD), the electrochemical impedance spectrum was tested in the frequency range of 100–10 MHz. Linear polarization curves were obtained by scanning the electrodes from -8 to 8 mV (vs. open circuit potential). The potential step measurements were tested at 100% charge state. A $+500 \text{ mV}$ potential was applied and the discharge time was 3600 s . For potential-step measurement, the electrodes in fully charged state were discharged with potential-steps of 0.5 V for 3600 s . The cut-off potential for all the above tests was 0.6 V versus Hg/HgO reference electrode and the testing temperature was 298 K .

3 Results and discussion

3.1 Microstructure

Figure 1 shows the typical Rietveld analysis pattern of $\text{La}_{0.5}\text{Nd}_{0.05}\text{Sm}_{0.3}\text{Mg}_{0.15}\text{Ni}_{3.5}$ alloy. Lattice parameters, cell volume and phase relative abundance of the alloys are listed in Table 1. The degree of the refinements is judged by s : $s = R_{\text{wp}}/R_e$, where R_{wp} is the weighed sum of residuals of the least square fit and R_e is the value statistically expected. It can be seen that the alloys have multiphase structure including the major A_2B_7 and A_5B_{19} phases and residual AB_5 phase. $\text{Pr}_5\text{Co}_{19}$ -type phase disappears after annealing treatment time prolonged to 9 h . Moreover, it can be found that a -axis parameter, c -axis and unit cell volume of the phases remain almost unchanged with prolonging the holding time. However, the abundance of A_2B_7 phase first increases and then decreases with increasing t value from 6 to 12 while A_5B_{19} and AB_5 phase abundance shows the reverse trend (Fig. 2).

Figure 3a shows SEM image of $\text{La}_{0.5}\text{Nd}_{0.05}\text{Sm}_{0.3}\text{Mg}_{0.15}\text{Ni}_{3.5}$ alloy annealed at 1048 K for 12 h . It is seen from SEM that the microstructure is mainly composed of A and B phases. From EDS it is found that A and B phases have different elemental compositions but the elements distributes evenly within each phase.

3.2 Activation capability and maximum discharge capability

The number of cycles (N_a) needed to activate the electrodes and maximum discharge capacity (C_{\max}) of $\text{La}_{0.5}\text{Nd}_{0.05}\text{Sm}_{0.3}\text{Mg}_{0.15}\text{Ni}_{3.5}$ alloy electrodes are given in Table 2. It is noted that all the alloys with different

annealing treatment time are easily activated to reach the maximum capacity within 2 cycles and show good activation property. However, the activation property of the alloy electrodes is not affected by prolonging annealing treatment time. The superior activation performances are mainly ascribed to the phase boundaries in the multiphase alloys, which can not only decrease the lattice distortion and the strain energy formed in the process of hydrogen absorption/desorption, but also provide tunnels for the diffusion of hydrogen atoms.

The maximum discharge capacities of alloy electrodes monotonically increase from 326.5 mAh g^{-1} ($t=6 \text{ h}$) to 362.2 mAh g^{-1} ($t=12 \text{ h}$). It is mainly ascribed to the increase of hydrogen storage phase abundance. It has been shown that Ce_2Ni_7 -type, Gd_2Co_7 -type, and $\text{Ce}_5\text{Co}_{19}$ -type phases present the increasing trend as a whole and possess higher hydrogen storage capacity than CaCu_5 -type phase [19, 20]. Also, Ce_2Ni_7 -type, Gd_2Co_7 -type, and $\text{Ce}_5\text{Co}_{19}$ -type phases as main phase play a dominant role in discharge capacity. PCT curves of $\text{La}_{0.5}\text{Nd}_{0.05}\text{Sm}_{0.3}\text{Mg}_{0.15}\text{Ni}_{3.5}$ alloys (Fig. 4) show that the hydrogen storage capacity increases, and the hysteresis becomes smaller and more flat with increasing t value. Moreover, the plateau pressure for hydrogen absorption–desorption gradually increases, which indicates that the stability of hydride reduces with lengthening annealing treatment time from 6 to 12 h . Therefore, prolonging annealing treatment time is beneficial to enhance discharge capacity of $\text{La}_{0.5}\text{Nd}_{0.05}\text{Sm}_{0.3}\text{Mg}_{0.15}\text{Ni}_{3.5}$ alloy electrodes.

3.3 High-rate dischargeability and electrochemical kinetics

Figure 5 shows the relationship between the high-rate dischargeability (HRD) and the discharge current density of $\text{La}_{0.5}\text{Nd}_{0.05}\text{Sm}_{0.3}\text{Mg}_{0.15}\text{Ni}_{3.5}$ alloy electrodes. HRD of the alloy electrodes increases with t decreasing from 12 to 6 h . HRD at the discharge current density of 2000 mA g^{-1} (HRD_{2000}) is listed in Table 2. HRD_{2000} monotonically decreases from 63.8% ($t=6 \text{ h}$) to 55.5% ($t=12 \text{ h}$).

To clarify the effect of annealing time on electrochemical kinetics of $\text{La}_{0.5}\text{Nd}_{0.05}\text{Sm}_{0.3}\text{Mg}_{0.15}\text{Ni}_{3.5}$ alloy electrodes, the exchange current density (i_0) and the hydrogen diffusion coefficient (D) are measured by using the potential step technique. i_0 is the rate of hydriding/dehydriding at the equilibrium state and can be used to evaluate electrocatalytic activity for charge-transfer reaction on the surface of alloy electrodes, as well as D characterizes the mass transport properties of an alloy electrode. [21].

The charge-transfer resistance at the surface of the alloys is determined by the electrochemical impedance spectrum (EIS). EIS of $\text{La}_{0.5}\text{Nd}_{0.05}\text{Sm}_{0.3}\text{Mg}_{0.15}\text{Ni}_{3.5}$ alloy electrodes at 50% DOD at 298 K is shown in Fig. 6. Kuriyama

Fig. 1 Reitveld analysis results of XRD for the $\text{La}_{0.5}\text{Nd}_{0.05}\text{Sm}_{0.3}\text{Mg}_{0.15}\text{Ni}_{3.5}$ alloys

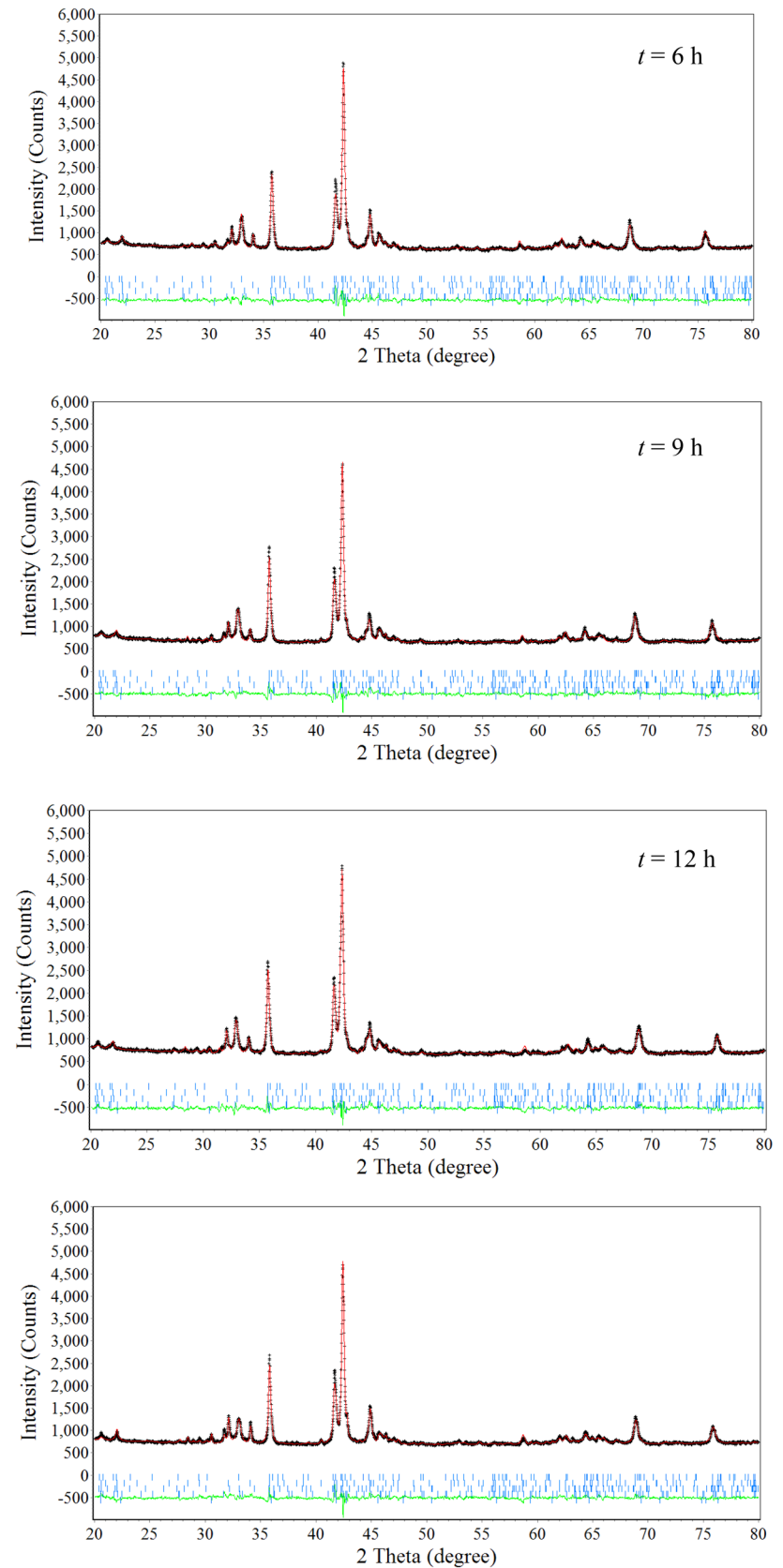
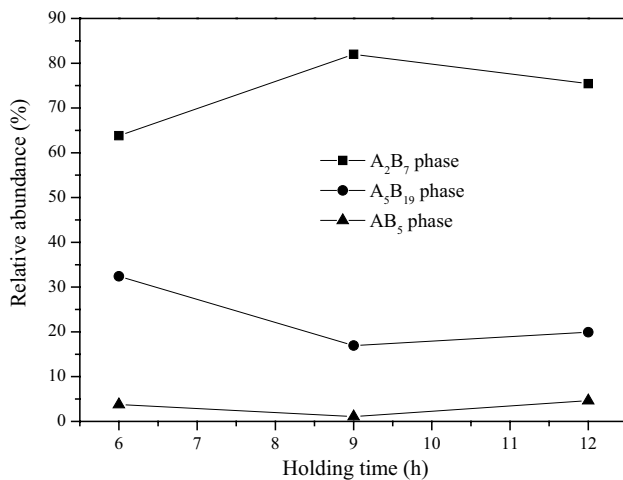


Table 1 Lattice parameter and phase abundance of $\text{La}_{0.5}\text{Nd}_{0.05}\text{Sm}_{0.3}\text{Mg}_{0.15}\text{Ni}_{3.5}$ alloys

Alloys	Str. type	a (Å)	c (Å)	V (Å ³)	Abundance (%)
$t = 6$ h					
$R_p = 2.64$	Ce_2Ni_7	5.0161	24.272	528.89	26.40
$R_{wp} = 3.56$	Gd_2Co_7	5.0157	36.335	791.62	37.41
	$\text{Pr}_5\text{Co}_{19}$	5.0207	32.497	709.44	9.81
	$\text{Ce}_5\text{Co}_{19}$	5.0114	48.335	1051.2	22.60
	CaCu_5	4.9880	3.9776	85.706	3.78
$t = 9$ h					
$R_p = 2.76$	Ce_2Ni_7	5.0189	24.289	529.88	29.15
$R_{wp} = 3.82$	Gd_2Co_7	5.0175	36.353	792.58	52.83
	$\text{Ce}_5\text{Co}_{19}$	5.0064	48.429	1051.2	16.93
	CaCu_5	4.9900	3.9755	85.730	1.09
$t = 12$ h					
$R_p = 2.80$	Ce_2Ni_7	5.0180	24.213	527.99	27.73
$R_{wp} = 3.86$	Gd_2Co_7	5.0137	36.322	790.71	47.71
	$\text{Ce}_5\text{Co}_{19}$	5.0104	48.297	1050.0	19.92
	CaCu_5	4.9879	3.9973	85.693	4.65

**Fig. 2** Evolution of the relative phase abundance of alloy versus the holding time

et al. [22]. ascribed the larger semicircle in the low frequency region to the charge-transfer resistance on the alloy surface, and the semicircle in high-frequency region to the contact resistance between the alloy powder and the conductive material. Therefore, the larger the radius of the semicircle in the low frequency region is, the larger the charge-transfer resistance of the alloy electrode will be. As shown in Fig. 6, the radius of the semicircle of $\text{La}_{0.5}\text{Nd}_{0.05}\text{Sm}_{0.3}\text{Mg}_{0.15}\text{Ni}_{3.5}$ alloy in the low-frequency and high-frequency remains almost unchanged with prolonging the annealing treatment time. On the basis of the circuit and by means of fitting program Z-VIEW, R_{ct} were obtained. Table 2 gave R_{ct} and I_0 obtained by the following equation [22]:

$$I_0 = (RT/F)(1/R_{ct}) \quad (2)$$

where R was the gas constant, T was the absolute temperature and F was the Faraday constant. The R_{ct} values of the alloy electrodes is 105.3 $\text{m}\Omega \text{g}$ ($t = 6$ h), 101.5 $\text{m}\Omega \text{g}$ ($t = 9$ h) and 103.7 $\text{m}\Omega \text{g}$ ($t = 12$ h), respectively. The I_0 values are calculated by Eq. (2) and listed in Table 3. It is clear that the variation of I_0 is 243.9 mA g^{-1} ($t = 6$ h), 253.0 mA g^{-1} ($t = 9$ h) and 247.6 mA g^{-1} ($t = 12$ h). This is to say, the annealing time plays a little role on the charge-transfer reaction of the alloy electrode, which may be ascribed to the little effect of annealing time on the surface state of the alloy electrode.

Figure 7 shows the semi-logarithmic plots of the anodic current versus the time response of $\text{La}_{0.5}\text{Nd}_{0.05}\text{Sm}_{0.3}\text{Mg}_{0.15}\text{Ni}_{3.5}$ alloy electrodes. It can be seen that the current–time responses can be divided into two time domains [23]. In the first time region, the oxidation current of hydrogen rapidly declines due to the rapid consumption of hydrogen on the surface. In the following time region, the current declines more slowly and drops linearly with time. Since hydrogen is supplied from the bulk of the alloy at a rate proportional to the concentration gradient of hydrogen, the electrode current is controlled by the diffusion of hydrogen in the second time region. Zheng et al. [23] reported that in a large anodic potential-step test, after a long discharge time, the diffusion current varies with time according to the following equation:

$$D = -\frac{2.3.3a^2}{\pi^2} \frac{d \lg i}{dt} \quad (3)$$

where i is anodic current density (A g^{-1}), D is the hydrogen diffusion coefficient ($\text{cm}^2 \text{s}^{-1}$), d is the density of the alloy

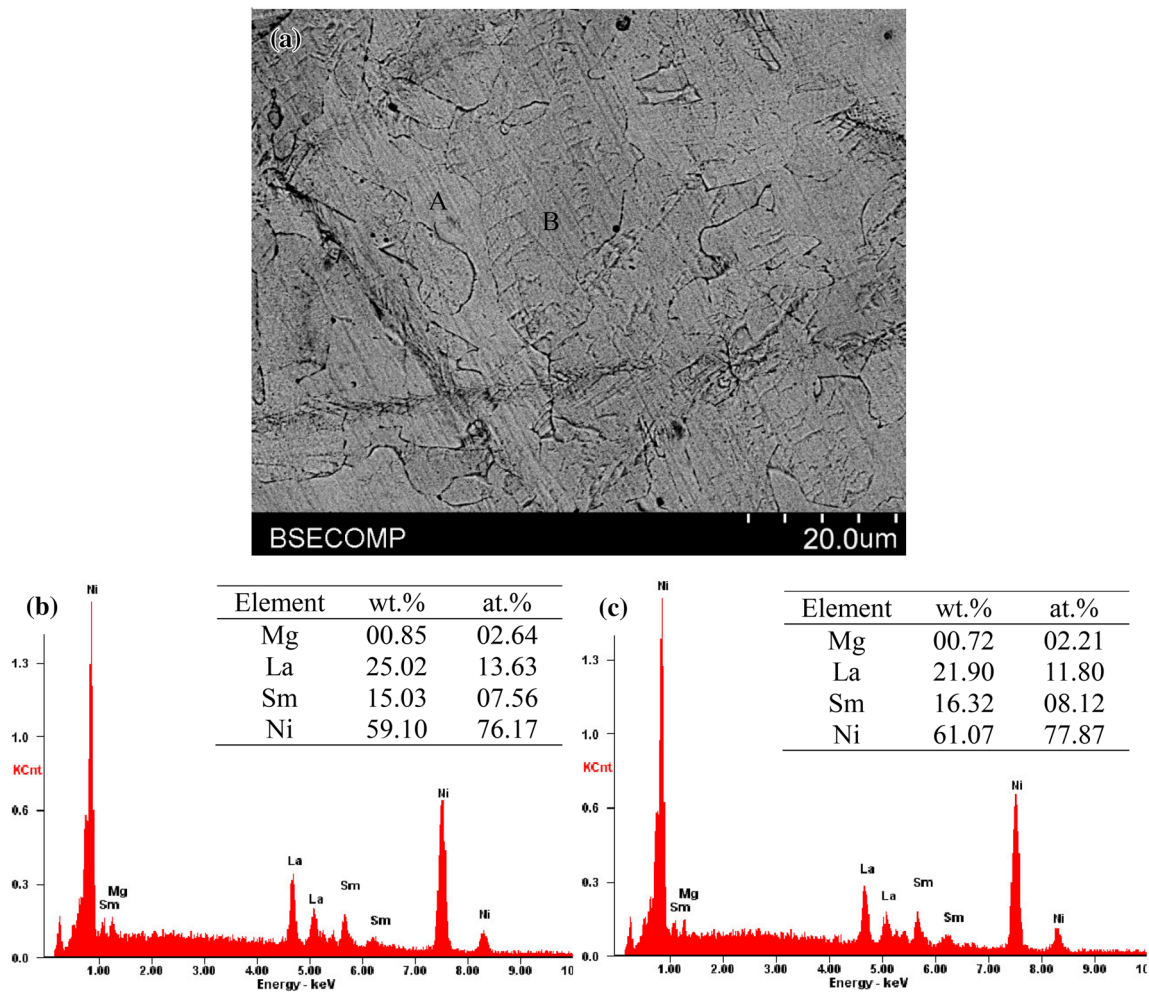


Fig. 3 SEM and EDS results of $\text{La}_{0.5}\text{Nd}_{0.05}\text{Sm}_{0.3}\text{Mg}_{0.15}\text{Ni}_{3.5}$ alloy annealed at 1048 K for 12 h **a** BSE **b** EDS of A area **c** EDS of B area

Table 2 Electrochemical performances of $\text{La}_{0.5}\text{Nd}_{0.05}\text{Sm}_{0.3}\text{Mg}_{0.15}\text{Ni}_{3.5}$ alloy electrodes

t (h)	C_{max} (mAh/g)	N_a^b	HRD ₂₀₀₀ ^a (%)	S_{200} (%)
6	326.5	2	63.8	67.0
9	340.5	2	60.5	68.6
12	362.2	2	55.5	70.6

^aThe high-rate dischargeability at the discharge current density of 2000 mA/g

^bThe number of cycles needed to activate the electrode

(g cm^{-3}), a is the radius of the alloy particle, C_0 is the initial hydrogen concentration in the bulk of the alloy (mol cm^{-3}), C_s is the surface hydrogen concentration of the alloy (mol cm^{-3}) and t is the discharge time (s). Assuming that the alloy has a similar particle distribution with an average particle radius of 13 μm according to previous study [24], D was calculated and summarized in Table 3. The D of

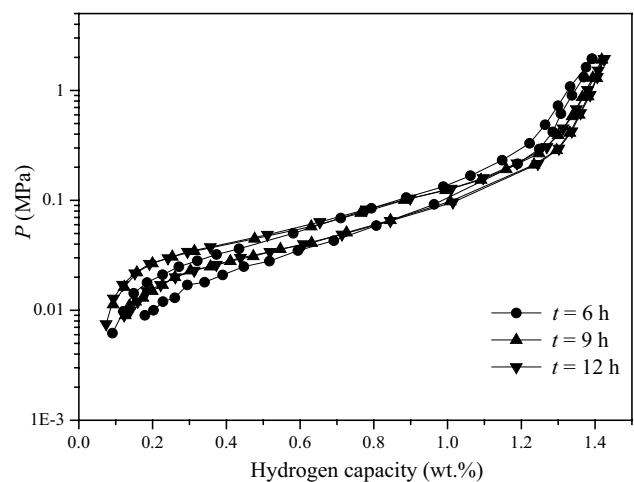


Fig. 4 PCT of $\text{La}_{0.5}\text{Nd}_{0.05}\text{Sm}_{0.3}\text{Mg}_{0.15}\text{Ni}_{3.5}$ alloy electrodes

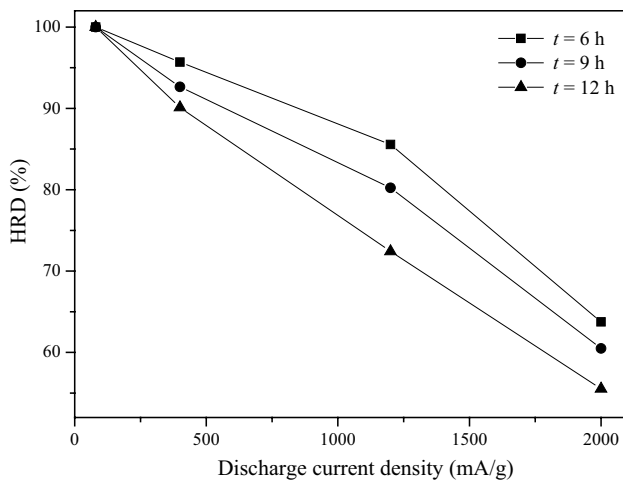


Fig. 5 HRD of La_{0.5}Nd_{0.05}Sm_{0.3}Mg_{0.15}Ni_{3.5} alloy electrodes

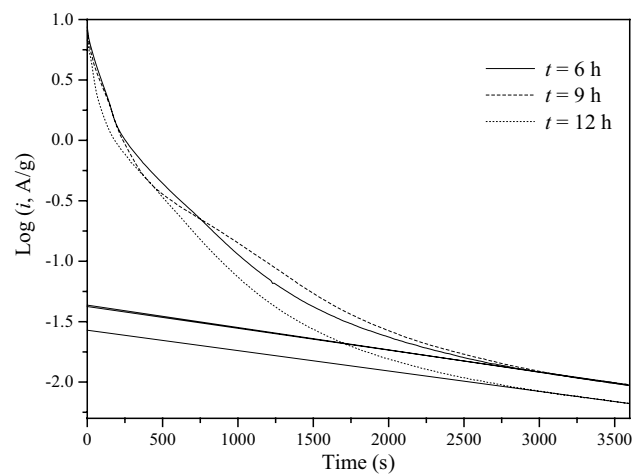


Fig. 7 Semilogarithmic curves of anodic current versus time of response of La_{0.5}Nd_{0.05}Sm_{0.3}Mg_{0.15}Ni_{3.5} alloy electrodes

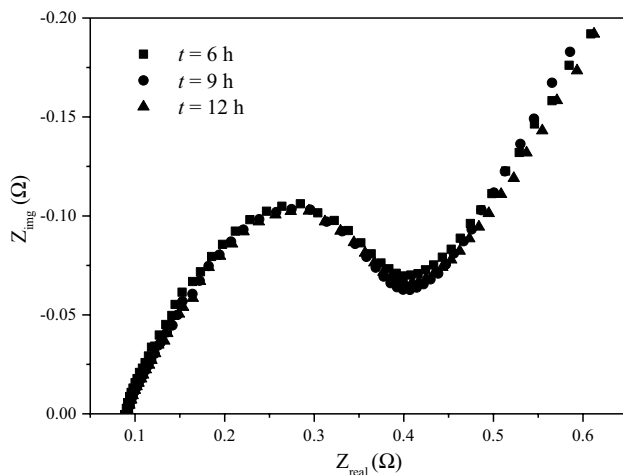


Fig. 6 EIS of La_{0.5}Nd_{0.05}Sm_{0.3}Mg_{0.15}Ni_{3.5} alloy electrodes at 50% DOD

Table 3 Electrochemical kinetic characteristics of La_{0.5}Nd_{0.05}Sm_{0.3}Mg_{0.15}Ni_{3.5} alloy electrodes

t (h)	R _p (mΩ g)	I ₀ (mA/g)	D (× 10 ⁻¹⁰ cm ² /s)
6	105.3	243.9	7.29
9	101.5	253.0	7.10
12	103.7	247.6	6.64

La_{0.5}Nd_{0.05}Sm_{0.3}Mg_{0.15}Ni_{3.5} alloy electrodes monotonically decrease from 7.29 × 10⁻¹¹ (t = 6 h) to 6.64 × 10⁻¹¹ cm² s⁻¹ (t = 12 h) with increasing t value. From the analyses above, lengthening annealing treatment time can deteriorate the hydrogen diffusion within the alloy bulk. The variation tendency of HRD is in agreement with change trend of the

hydrogen diffusion coefficient (D) with increasing t value, which indicate that the hydrogen diffusion ability in the alloy bulk is the predominance factors of the electrochemical kinetics of the alloy electrodes.

3.4 Cycling stability

Cycling stability is an extremely important factor for the service life of hydrogen storage alloys. It is expressed by the cycling capacity retention rate S_n which can be calculated by the following formula:

$$S_n = \frac{C_n}{C_{max}} \times 100\% \tag{4}$$

where C_n is the discharge capacity at the nth charging/discharging cycle and C_{max} is the maximum discharge capacity with a current density of 80 mA/g. The slopes of the cycling capacity retention rate versus as cycle number as shown in Fig. 8 represent the degradation rate of the discharge capacity during the charging/discharging cycle. The smaller slope value means better cycle stability of the alloy. It can be seen that the curve slopes of the alloys become slightly smaller with increasing annealing treatment time, which suggests that lengthening annealing treatment time can enhance the cycle stability of the alloy. In addition, the capacity retaining rate S₂₀₀ of the alloy electrodes at 200th charging–discharging cycle as a function of Sm content are also listed in Table 2. It can be seen that S₂₀₀ monotonically increases from 67.0% (t = 6 h) to 70.6% (t = 12 h), which indicates that the lengthening annealing treatment time can improve the cycle stability of the alloy electrodes. The improvement of cycling

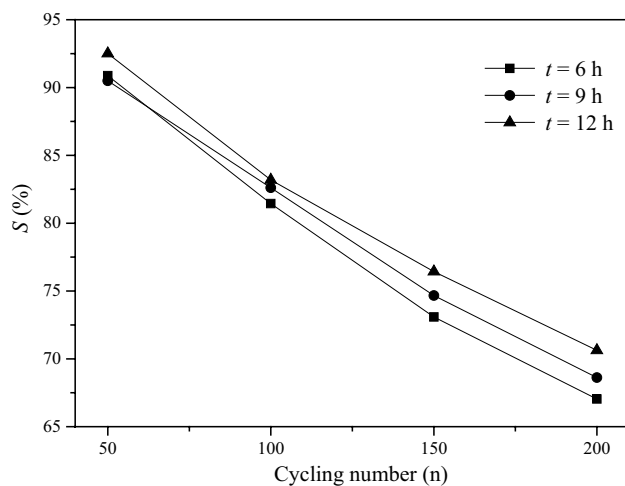


Fig. 8 Cycling stability of $\text{La}_{0.5}\text{Nd}_{0.05}\text{Sm}_{0.3}\text{Mg}_{0.15}\text{Ni}_{3.5}$ alloy electrodes

stability should be ascribed to the more homogeneous microstructure with increasing annealing time.

4 Conclusions

In this paper, $\text{La}_{0.5}\text{Nd}_{0.05}\text{Sm}_{0.30}\text{Mg}_{0.15}\text{Ni}_{3.5}$ alloy was prepared by induction melting followed by annealing treatments at 1048 K for 6 h, 9 h and 12 h, respectively. The effects of the annealing time on the microstructure and electrochemical performances of the alloys were systematically investigated. The following conclusions can be drawn:

1. Rietveld analyses pattern shows that the alloys have multiphase structure including the major A_2B_7 and A_5B_{19} phases and residual AB_5 phase. $\text{Pr}_5\text{Co}_{19}$ -type phase disappears after annealing treatment time prolonged to 9 h. Moreover, a -axis parameter, c -axis and unit cell volume of the phases remain almost unchanged with prolonging the holding time. However, the abundance of the A_2B_7 phase first increases and then decreases with increasing time value from 6 to 12 h while A_5B_{19} phase and the AB_5 phase abundance shows the reverse trend.
2. The activation property of the as-annealed alloy electrodes is improved. However, the activation property of the alloy electrodes is not affected by prolonging annealing treatment time. The maximum discharge capacity of alloy electrodes first increase from 326.5 mA/g ($t = 6$ h) to 362.2 mA/g ($t = 12$ h) with increasing t value.

3. HRD_{2000} decreases from 63.8% ($t = 6$ h) to 55.5% ($t = 12$ h), which is determined by the hydrogen diffusion coefficient.
4. The cycling capacity retention rate at the 200th cycle monotonically increases from 67.0% ($t = 6$ h) to 70.6% ($t = 12$ h).

Funding This work was financially supported by Innovation Fund of Inner Mongolia University of Science and Technology (2017QDL-B02) and Natural Science Foundation of Inner Mongolia (2018BS05010).

Compliance with ethical standards

Conflict of interest The authors declare that they have no conflicts of interest.

References

1. Ouyang LZ, Yang XS, Zhu M, Liu JW, Dong HW, Sun DL, Zou J, Yao XD (2014) Enhanced hydrogen storage kinetics and stability by synergistic effects of in situ formed $\text{CeH}_{2.73}$ and Ni in $\text{CeH}_{2.73}\text{MgH}_2$ Ni nanocomposites. *J Phys Chem C* 118:7808–7820. <https://doi.org/10.1021/jp500439n>
2. Reilly JJ, Adzic GD, Johnson JR, Vogt T, Mukerjee S, McBreen J (1999) The correlation between composition and electrochemical properties of metal hydride electrodes. *J Alloy Compd* 293–295:569–582. [https://doi.org/10.1016/S0925-8388\(99\)00413-2](https://doi.org/10.1016/S0925-8388(99)00413-2)
3. Liu YF, Pan HG, Zhu YF, Li R, Lei YQ (2004) Influence of Mn content on the structural and electrochemical properties of the $\text{La}_{0.7}\text{Mg}_{0.3}\text{Ni}_{4.25-x}\text{Co}_{0.75}\text{Mn}_x$ hydrogen storage alloys. *Mater Sci Eng A* 372:163–172. <https://doi.org/10.1016/j.msea.2003.12.004>
4. Cao ZJ, Ouyang LZ, Wang H, Liu JW, Sun DL, Zhang QA, Zhu M (2014) Structural characteristics and hydrogen storage properties of Sm_2Co_7 . *J Alloy Compd* 608:14–18. <https://doi.org/10.1016/j.jallcom.2014.04.106>
5. Ouyang LZ, Cao ZJ, Li LL, Wang H, Liu JW, Min D, Chen YW, Xiao FM, Tang RH, Zhu M (2014) Enhanced high-rate discharge properties of $\text{La}_{11.3}\text{Mg}_{6.0}\text{Sm}_{7.4}\text{Ni}_{61.0}\text{Co}_{7.2}\text{Al}_{7.1}$ with added graphene synthesized by plasma milling. *Int J Hydrog Energy* 39:12765–12772. <https://doi.org/10.1016/j.ijhydene.2014.06.111>
6. Ouyang Liuzhang, Yang Tonghan, Zhu Min, Min De, Luo Tongzhao, Wang Hui, Xiao Fangming, Tang Renheng (2018) Hydrogen storage and electrochemical properties of Pr, Nd and Co-free $\text{La}_{13.9}\text{Sm}_{24.7}\text{Mg}_{1.5}\text{Ni}_{58}\text{Al}_{1.7}\text{Zr}_{0.14}\text{Ag}_{0.07}$ alloy as a nickel–metal hydride battery electrode. *J. Alloys Compd* 735:98–103. <https://doi.org/10.1016/j.jallcom.2017.10.268>
7. Cao Zhijie, Ouyang Liuzhang, Li Lingling, Yanshan Lu, Wang Hui, Liu Jiangwen, Min De, Chen Yanwen, Xiao Fangming, Sun Tai, Tang Renheng, Zhu Min (2015) Enhanced discharge capacity and cycling properties in high-samarium, praseodymium/neodymium-free, and low-cobalt A_2B_7 electrode materials for nickel–metal hydride battery. *Int J Hydrog Energy* 40:451–455. <https://doi.org/10.1016/j.ijhydene.2014.11.016>
8. Kohno T, Yoshida H, Kawashima F, Inaba T, Sakai I, Yamamoto M, Kanda M (2000) Hydrogen storage properties of new ternary system alloys: La_2MgNi_9 , $\text{La}_5\text{Mg}_2\text{Ni}_{23}$, $\text{La}_3\text{MgNi}_{14}$. *J Alloy Compd* 311:L5–L7. [https://doi.org/10.1016/S0925-8388\(00\)01119-1](https://doi.org/10.1016/S0925-8388(00)01119-1)
9. Gao Zhijie, Kang Long, Luo Yongchun (2013) Microstructure and electrochemical hydrogen storage properties of

- La–Mg–Ni-based alloy electrodes. *New J Chem* 37:1105–1114. <https://doi.org/10.1039/C3NJ41044G>
- Li Rongfeng, Peizhen Xu, Zhao Yamin, Wan Jing, Liu Xiaofang, Ronghai Yu (2014) The microstructures and electrochemical performances of $\text{La}_{0.6}\text{Gd}_{0.2}\text{Mg}_{0.2}\text{Ni}_{3.0}\text{Co}_{0.5-x}\text{Al}_x$ ($x=0-0.5$) hydrogen storage alloys as negative electrodes for nickel/metal hydride secondary batteries. *J Power Sour* 270:21–27. <https://doi.org/10.1016/j.jpowsour.2014.07.092>
 - Liu Yongfeng, Cao Yanhui, Huang Li, Gao Mingxia, Pan Hongge (2011) Rare earth–Mg–Ni-based hydrogen storage alloys as negative electrode materials for Ni/MH batteries. *J Alloy Compd* 509(3):675–686. <https://doi.org/10.1016/j.jallcom.2010.08.157>
 - Liu Yongfeng, Pan Hongge, Gao Mingxia, Wang Qidong (2011) Advanced hydrogen storage alloys for Ni/MH rechargeable batteries. *J Mater Chem* 21:4743–4755. <https://doi.org/10.1039/C0JM01921F>
 - Sakai T, Miyamura H, Kuriyama N, Ishikawa H, Uehara I (1994) Hydrogen storage alloys for nickel–metal hydride battery. *Z Phys Chem* 183:333–346. https://doi.org/10.1524/zpch.1994.183.Part_1_2.333
 - Hua Wei-Kang, Denysa Roman V, Nwakwuo Christopher C, Holm Thomas, Maehlen Jan Petter, Solberg Jan Ketil, Yartys Volodymyr A (2013) Annealing effect on phase composition and electrochemical properties of the Co-free La_2MgNi_9 anode for Ni–metal hydride batteries. *Electrochim Acta* 96:27–33. <https://doi.org/10.1016/j.electacta.2013.02.064>
 - Jiang Weiqing, Mo Xiaohua, Guo Jin, Wei Yinyan (2013) Effect of annealing on the structure and electrochemical properties of $\text{La}_{1.8}\text{Ti}_{0.2}\text{MgNi}_{8.9}\text{Al}_{0.1}$ hydrogen storage alloy. *J Power Sour* 221:84–89. <https://doi.org/10.1016/j.jpowsour.2012.08.022>
 - Pan Hongge, Liu Yongfeng, Gao Mingxia, Zhu Yunfeng, Lei Yongquan, Wang Qidong (2003) A study on the effect of annealing treatment on the electrochemical properties of $\text{La}_{0.67}\text{Mg}_{0.33}\text{Ni}_{2.5}\text{Co}_{0.5}$ alloy electrodes. *Int J Hydrog Energy* 28:113–117. [https://doi.org/10.1016/S0360-3199\(02\)00035-6](https://doi.org/10.1016/S0360-3199(02)00035-6)
 - Pan Hongge, Chen Ni, Gao Mingxia, Li Rui, Lei Yongquan, Wang Qidong (2005) Effects of annealing temperature on structure and the electrochemical properties of $\text{La}_{0.7}\text{Mg}_{0.3}\text{Ni}_{2.45}\text{Co}_{0.75}\text{Mn}_{0.1}\text{Al}_{0.2}$ hydrogen storage alloy. *J Alloy Compd* 397:306–312. <https://doi.org/10.1016/j.jallcom.2005.01.040>
 - Wang Beiping, Chen Yuanzhen, Wang Li, Liu Yongning (2012) Effect of annealing time on the structure and electrochemical properties of $\text{La}_{0.72}\text{Nd}_{0.08}\text{Mg}_{0.2}\text{Ni}_{3.4}\text{Al}_{0.1}$ hydrogen storage alloys. *J Alloy Compd* 541:305–309. <https://doi.org/10.1016/j.jallcom.2012.06.052>
 - Dunlap BD, Viccaro PJ, Shenoy GK (1980) Structural relationships in rare earth–transition metal hydrides. *J Less Common Metals* 74:75–79. [https://doi.org/10.1016/0022-5088\(80\)90075-2](https://doi.org/10.1016/0022-5088(80)90075-2)
 - Ozaki T, Kanemoto M, Takeya T, Kitano Y, Kuzuhara M, Watada M, Tanase S, Sakai T (2007) Stacking structures and electrode performances of rare earth–Mg–Ni-based alloys for advanced nickel–metal hydride battery. *J Alloy Compd* 446–447:620–624. <https://doi.org/10.1016/j.jallcom.2007.03.059>
 - Pan Hongge, Ma Jianxin, Wang Chunsheng, Chen Shaoan, Wang Xinghua, Chen Changpin, Wang Qidong (1999) Studies on the electrochemical properties of $\text{MgNi}_{4.3-x}\text{Co}_x\text{Al}_{0.7}$ hydride alloy electrodes. *J Alloy Compd* 293–295:648–652. [https://doi.org/10.1016/S0925-8388\(99\)00359-X](https://doi.org/10.1016/S0925-8388(99)00359-X)
 - Kuriyama Nobuhiro, Sakai Tetsuo, Miyamura Hiroshi, Uehara Itsuki, Ishikawa Hiroshi, Iwasaki Toshikatsu (1993) Electrochemical impedance and deterioration behavior of metal hydride electrodes. *J Alloy Compd* 202:183–197. [https://doi.org/10.1016/0925-8388\(93\)90538-X](https://doi.org/10.1016/0925-8388(93)90538-X)
 - Zheng G, Popov BN, White RE (1995) Electrochemical determination of the diffusion coefficient of hydrogen through a $\text{LaNi}_{4.25}\text{Al}_{0.75}$ electrode in alkaline aqueous solution. *J Electrochem Soc* 142:2695–2698. <https://doi.org/10.1149/1.2050076>
 - Liu Baozhong, Fan Guangxin, Wang Youchao, Mi Guofa, Yaoming Wu, Wang Limin (2008) Crystallographic and electrochemical characteristics of melt-spun Ti–Zr–Ni–Y alloys. *Int J Hydrog Energy* 33:5801–5806. <https://doi.org/10.1016/j.ijhyene.2008.07.043>